An Active Concentric Electrode for Concurrent EEG Recording and Body-Coupled Communication (BCC) Data Transmission

Tao Tang, *Member, IEEE*, Long Yan, *Senior Member, IEEE*, Jeong Hoan Park, *Member, IEEE*, Han Wu, *Student Member, IEEE*, Lian Zhang, *Student Member, IEEE*, Jiamin Li, *Student Member, IEEE*, Yilong Dong, *Student Member, IEEE*, Benjamin Ho Yin Lee, *Student Member, IEEE*, and Jerald Yoo, *Senior Member, IEEE*

***Abstract*—This paper presents a wearable active concentric electrode for *concurrent* EEG monitoring and Body-Coupled Communication (BCC) data transmission. A three-layer concentric electrode eliminates the usage of wires. A common mode averaging unit (CMAU) is proposed to cancel not only the continuous common-mode interference (CMI) but also the instantaneous CMI of up to 51V_{pp}. The localized potential matching technique removes the ground electrode. An open-loop programmable gain amplifier (OPPGA) with the pseudo-resistor-based RC-divider block is presented to save the silicon area. The presented work is the first reported so far to achieve the concurrent EEG signal recording and BCC-based data transmission. The proposed chip achieves 100 dB CMRR and 110 dB PSRR, occupies 0.044 mm^2, and consumes 7.4 μW with an input-referred noise density of 26 nV/$\sqrt{\text{Hz}}$.**

***Index Terms*—Active electrode, concentric electrode, common-mode interference, common-mode averaging, concurrent recording/transmitting, EEG recording, instantaneous common-mode interference rejection, localized potential matching.**

I. Introduction

EEG RECORDING creates an opportunity to sense human brain activity in a non-invasive manner [1]–[4]. Quantitative EEG analysis or brain mapping, which is based on multiple EEG sensing channels, provides the patient's mental and physiological information for monitoring purposes. However, conventional multi-channel EEG requires various wire connections, making it difficult to be portable/wearable. The wearable EEG environment also suffers from environmental/common-mode interference (CMI), such as 50/60 Hz power line coupling, making it even more challenging for daily EEG monitoring. In particular, a wearable environment faces continuous CMI and instantaneous CMI (that happens, for example, when touching the laptop case or pulling the power plug), which must be addressed to achieve stable monitoring in daily life.

In efforts to mitigate such huge common-mode environmental interference, the works [5], [6] claimed that improving the CMRR from the instrumentation amplifier (IA) was the key. The work in [5] improved the IA's CMRR to be more than 115 dB by using tunable capacitors to compensate for the mismatches. [6] boosted the IA's CMRR by common-mode feedback (CMFB) circuit. Also, [7] developed a ping-pong auto zeroing and chopper-stabilized IA to achieve a CMRR of 140 dB. Although the reported CMRR was theoretically high enough to suppress CMI of up to 51V_{pp}, the work in [8] derived the CMRR relationship for a multi-channel system. Even with a more than 100 dB CMRR for the IA itself, the *system-level* CMRR can be as low as 60 dB for a multi-channel application. Therefore, previous works tried to compensate for the CMRR degradation from a system-level perspective. The system-level CMFB [9] or system-level common-mode feedforward (CMFF) [10] technique was proposed, which required extra hardware resources and consumed additional power. To improve system-level CMRR, the driven-right leg (DRL) circuit [11] could be used, but at the cost of system instability. Dedicated DRL works [12]–[15] tried to stabilize the system, but the extra DRL electrode coupled additional powerline interference and was inconvenient for wearable devices. The work in [16] discovered the imbalanced load issue and proposed an inverter-based preamp to solve the problem, while the other work [17] presented a TDM-based modulation scheme to obtain a balanced structure for multi-channel input. The reported works in [16], [17] improved the system-level CMRR to be more than 80 dB at the cost of additional preamp stages or fuzzy control strategies.

Besides improving the CMRR or solving the imbalanced load problem, reducing the number of transmission wire was

Manuscript received July 20, 2020; revised October 1, 2020; accepted November 4, 2020. Date of publication November 20, 2020; date of current version December 30, 2020. This work was supported in part by the A∗STAR AME Nanosystems at the Edge Program under Grant A18A4b0055, and in part by Hybrid Flexible Electronic Systems (HiFES) program, National University of Singapore under Grant R-263-501-011-133/731. *(Corresponding author: Jerald Yoo.)*

Tao Tang, Han Wu, Lian Zhang, Jiamin Li, Yilong Dong, and Benjamin Ho Yin Lee are with the National University of Singapore, Singapore 119077, Singapore (e-mail: elett@nus.edu.sg; wuhan@nus.edu.sg; lian.zhang@u.nus.edu; jiamin.li@u.nus.edu; ydong@u.nus.edu; benjamin_lee_ho_yin@u.nus.edu).

Long Yan is with the Samsung Electronics, Hwaseong 18448, Korea (e-mail: yanlong.ee@gmail.com).

Jeong Hoan Park was with the Department of Electrical and Computer Engineering, National University of Singapore, Singapore 117583, Singapore. He is now with Samsung Electronics, Hwaseong 18200, South Korea (e-mail: jh920.park@samsung.com).

Jerald Yoo is with the National University of Singapore, Singapore 117585, Singapore, and also with the N.1 Institute for Health, Singapore 117456, Singapore (e-mail: jyoo@nus.edu.sg).

Color versions of one or more of the figures in this article are available at https://doi.org/10.1109/TBCAS.2020.3039353.

Digital Object Identifier 10.1109/TBCAS.2020.3039353

another method to effectively suppress the CMI. The work in [18] proposed an active electrode concept to remove the transmission wire between the chip and electrodes. However, the cables between the recording electrode and reference electrode, and the ground electrode wire still existed and coupled a huge amount of CMI from the environment. The work in [19] proposed a charge pump technique to reduce the ground electrode's use, so the number of wires was further reduced; this method successfully compensated for the continuous CMI, but the charge pump would not be fast enough to compensate for the instantaneous CMI.

The silicon area of the AFE is another important issue for a multi-channel recording system because it directly determines the number of channels integrated into one chip; the works [2], [20], [21] reported to shrink the size of the IA with various techniques. The work in [2] proposed a group-chopping technique so that the open-loop amplifier could be used while minimizing the between-channel gain mismatch, and the work in [20] utilized an intrinsic capacitance as a feedback capacitor to save the silicon area. The work in [21] proposed an orthogonal chopping scheme for the inputs of 15 channels to share the same IA. Therefore, the area per channel was dramatically reduced. However, all of these works focused on the area of first stage IA, while the second stage of the AFE, normally the programmable gain amplifier (PGA), still occupied a large area due to the function of programmable gain.

Human biological data security is yet another important issue when designing wearable bio-potential recording devices. To achieve wireless transmitting among electrodes, the work [22] tried to send the information to each electrode by Bluetooth, which was power hungry and could be hacked for illegal purposes. The body channel communication (BCC) [23]–[32] provided a power-efficient and secure interface for data transmission through the user's body so that data security was well maintained. Moreover, when the human body was used as a communication interface, the transmission power was reduced compared with radio wave communication for wearable devices [29]–[30]. The work [31] tried to develop a human body model to optimize the BCC transceiver's power, and previous work proposed a mask-shaping technique to suppress interference with biological signals [32]. The work in [25] presented the integration of recording and BCC in a System-on-Chip (SoC). However, the concurrent recording/transmitting was not verified yet; to acquire the real-time data by the BCC technique, the system must transmit the bio-potential data while concurrently recording it.

To overcome the design difficulties mentioned above, we propose a concurrent EEG recording/transmitting wireless active concentric electrode [33].

II. The Proposed Active Concentric Electrode

The proposed active concentric electrode is shown in Fig. 1. This is the first distributed EEG recording system with BCC-based concurrent recording/transmitting reported so far.

A. Active Concentric Electrode Architecture

There are two functions in each sensor node: 1) EEG signal recording; 2) digitized EEG data transmission. In the recording part, the EEG signal is captured by the active concentric electrode's inner layer. The proposed two-stage open-loop programmable gain amplifier (OPPGA) amplifies the signal, and followed by a 10-bit SAR ADC for digitization. The environmental continuous and instantaneous CMI, which is up to $51\mathrm{V_{pp}}$, is dynamically suppressed by a common mode averaging unit (CMAU). The CMAU's output is directly connected to the chip's ground, as shown in Fig. 1, which is defined as the ground node for all blocks. In the data transmission part, the TX/RX can be alternatively selected for data transmission/receiving with the body channel communication (BCC) technique. An on-board trace (equivalent model of a 75 nH inductance $\mathrm{L_{parasitic}}$) couples the TX/RX signals to the chip's ground and transmits it to the transmission layer. The OOK-based TX is used to transmit data to another active concentric electrode for the average montage. Once the RX block in each active concentric electrode is enabled to receive data, the two electrodes can communicate with each other. An active concentric electrode is proposed to integrate the two functions, as shown in Fig. 1. Data is transmitted using the outer layer while the internal round area is used for EEG recording; an isolation gap is filled between the two layers. For an average montage, the common reference in the recorded signals is obtained from all active concentric electrodes. By combining recording and transmission, the ground electrode and transmission wires are removed. This allows for a secure bio-data delivery within the user's human body during EEG recording. The measured EEG data can be recorded and transmitted via BCC to the user's electrode which is integrated into the wearable devices, so the user's privacy is protected by the localized data transmission method.

In this active concentric electrode, the ground electrode has been removed by the localized potential matching technique. Additionally, the active concentric electrode is used to reduce the transmission wire from the working electrode. Therefore, the number of transmission wires has been reduced to the minimal. The coupled CMI from the environment has been reduced to the minimum as well.

The innovative concept of the active concentric electrode is utilizing a wide-bandwidth (1 Hz to 50 M Hz) concurrently. The EEG signal (normally less than 100 Hz) is located in the baseband, while the chopping stabilization, which is necessary for reducing flicker noise in the IA part, occupies the bandwidth of 2 to 10 k Hz, and the BCC TX transmission signal is modulated at 10 to 50 M Hz. The use of full-bandwidth operation dramatically

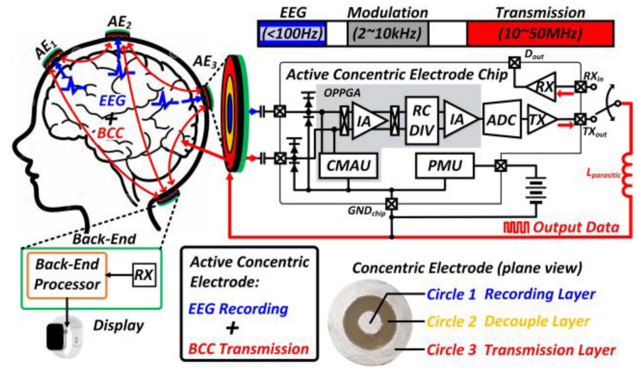

Fig. 1. System architecture of the active concentric electrode.

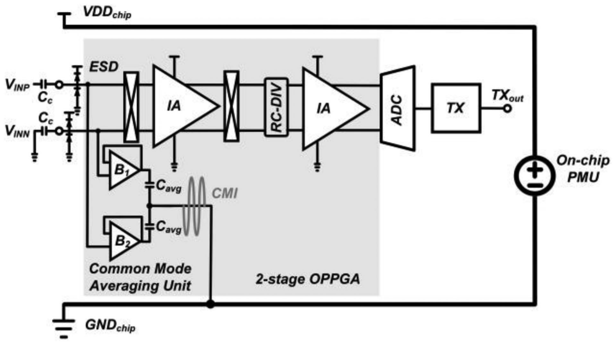

Fig. 2. Schematic of the proposed AFE.

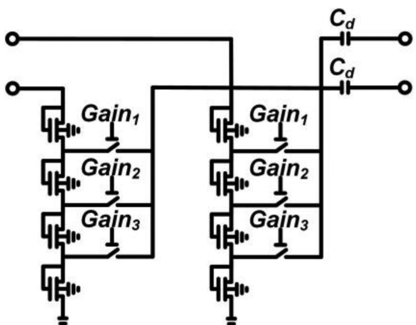

Fig. 3. Schematic of the RC-DIV.

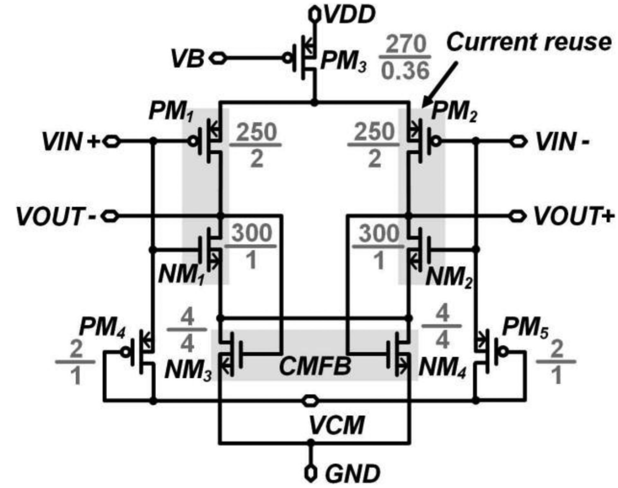

Fig. 4. Schematic of RC-free open loop amplifier and sizing of transistors.

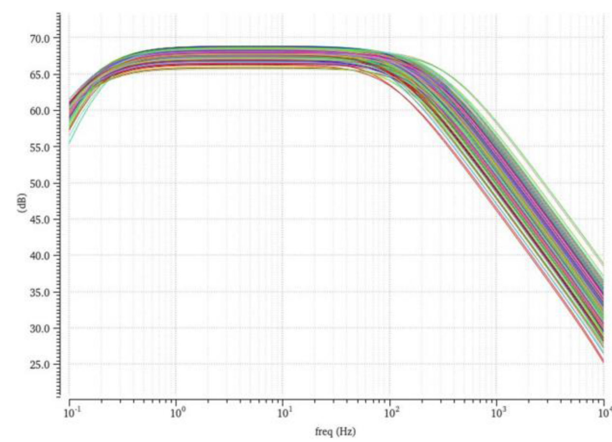

Fig. 5. Monte Carlo simulation of gain and bandwidth of the OPPGA.

reduces the need for transmission wires. Since the spectrum distance of the EEG signal, chopping stabilization, and BCC TX transmission is wide enough, the active concentric electrode achieves concurrent recording/transmitting without crosstalk of any signal.

B. Open-Loop Programmable Amplifier (OPPGA)

The schematic of the proposed AFE is shown in Fig. 2. To save the silicon area, a two-stage open-loop programmable gain amplifier (OPPGA) has been implemented. The proposed AFE consists of a 2-stage OPPGA, 10-bit ADC, TX, and on-chip PMU. The CMAU output is directly connected with the chip ground (GND_{chip}). Two averaging capacitors (C_{avg} in Fig. 2) average out the CMI and pass it to the ground (GND_{chip}). Conventional open-loop amplifiers [34], [35] with fixed gain are not suitable for bio-potential signal acquisition. A pseudo-resistor-based RC-divider (RC-DIV) block is developed to provide programmable gain, as shown in Fig. 3. Hence, the open-loop gain can be adjusted without any extra capacitor bank. Moreover, the pseudo resistor in the RC-DIV together with the small coupling capacitor C_d (3pF), forms a low -3 dB corner of 140/104/102 Hz for high/mid/low gain setting, respectively, which helps to filter out the unwanted chopping ripples from the first stage and transmission signal when TX for BCC is on, only leaving the recorded EEG signal for the second-stage amplification. Therefore, the RC-DIV unit provides two functions of both programmable gain and low-pass filtering, which saves significant area. The schematic of the IA is shown in Fig. 4. The proposed IA adopts the open-loop gain amplifier consuming only 2.1 μW while occupying 0.017 mm^2. The current-reuse technique is employed at the input stage to obtain high transconductance, which reduces the thermal noise floor with minimum current consumption. The transistor size (W/L) is listed in Fig. 4, where the two input transistor pairs (PM_1/NM_1 and PM_2/NM_2) are biased in a weak inversion region to maximize the transconductance efficiency. Transistors NM3 and NM4 provide the common-mode feedback to fix the output DC level. In contrast, two PMOS transistors (PM_4 and PM_5) are chosen as pseudo resistors to set the DC bias for the inputs, occupying a much smaller on-chip area than CMFB or other techniques. Two 100nF decoupling capacitors (Cc) are put in front of the choppers to ensure rail-to-rail DC offset cancellation. The Monte Carlo simulation result of the gain and bandwidth of the OPPGA is shown in Fig. 5. The gain/bandwidth variation, which is shown in Fig. 5, can be calibrated at the back-end to save the on-chip silicon area.

C. Common Mode Averaging Unit (CMAU)

There are considerable environmental interference, especially the 50/60 Hz powerline interference, as the main hazard for the recording AFE in the active concentric electrode. Techniques should be developed to suppress such huge instantaneous CMI. The work [19] proposed a common mode charge pump (CMCP)

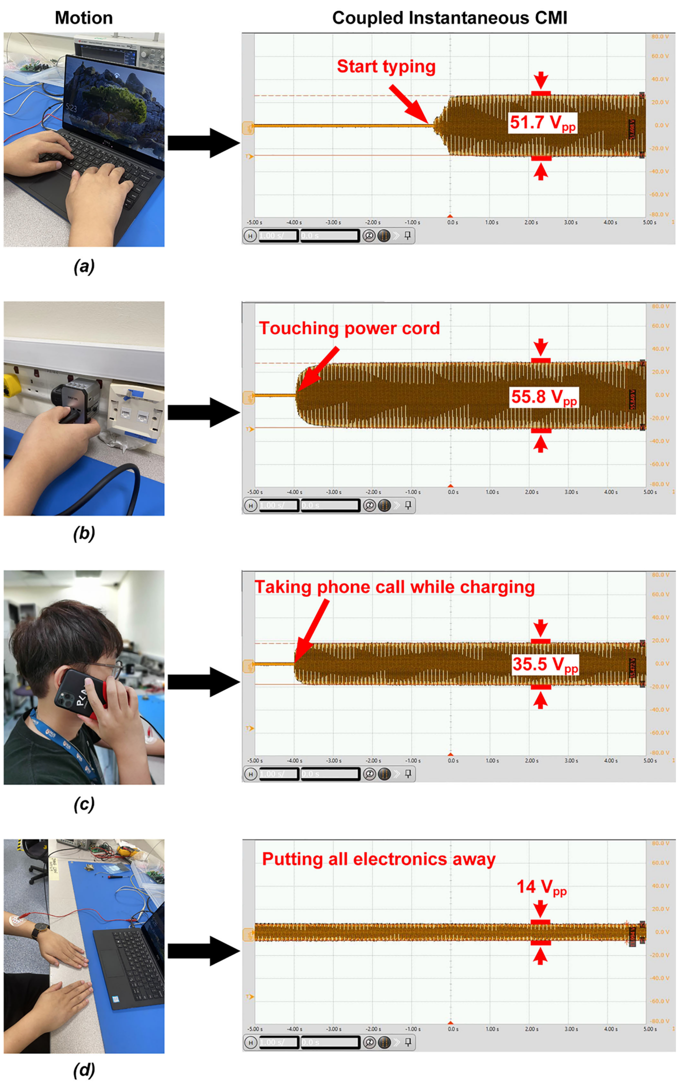

Fig. 6. Instantaneous/Continuous CMI coupling in daily life: (a) typing on a laptop; (b) unplugging power; (c) making phone call while charging; (d) leaving all electronics away.

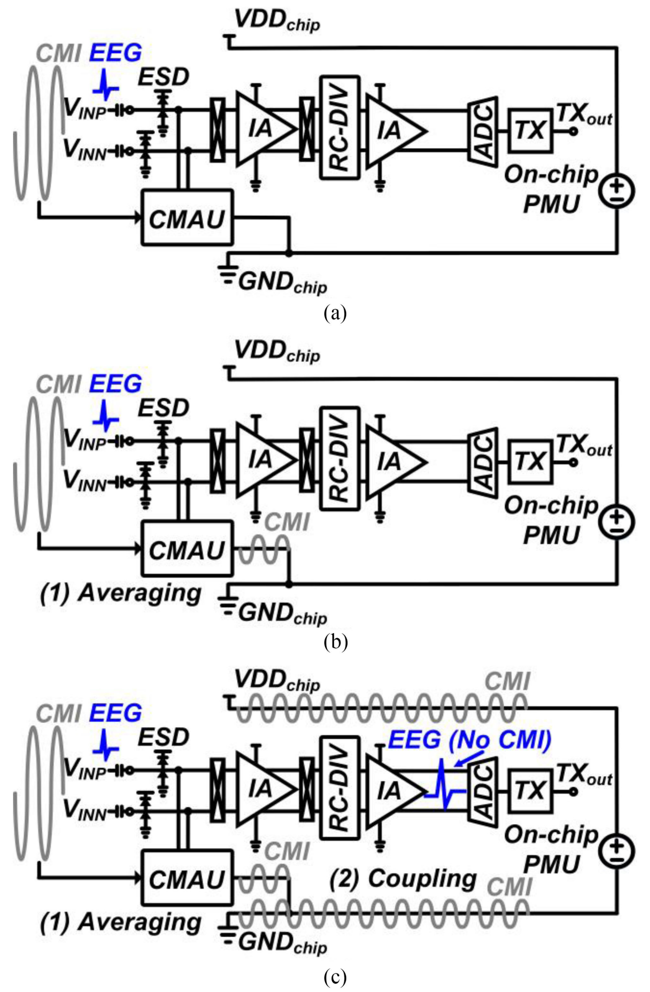

Fig. 7. Working principle of CMAU: (a) CMI and EEG coming in; (b) CMI averaging in CMAU; (c) averaged CMI coupling to circuit supply rails.

technique to suppress the common mode interference from power line coupling, while cancelling out a certain amount of common mode voltage. However, when the coupled common mode potential changes over time and environment, the capacitor's charging speed will be the bottleneck of the reported design. Another work [36] proposed the floating power system with an on-chip power unit. However, the floating power system is designed for multi-channel neural recording applications, and all channels are tied together to average out the common-mode potential, which is not suitable for a widespread distributed EEG recording system.

To quantify the amount of possible instantaneous/continuous CMI coupled to our body in daily life, a CMI coupling experiment was done to discover the dynamic change of the CMI. In this experiment, an electrode is attached to a subject's left arm and connected to the oscilloscope to show the amount of CMI. As shown in Fig. 6, when the subject is typing on a laptop, the coupled CMI is $51.7V_{pp}$ while touching the power cord to unplug the power, showing the coupled CMI suddenly changed to $55.8V_{pp}$. The CMI suddenly changes to $35.5V_{pp}$ when the subject makes a phone call (the phone is connected to a charger). Finally, the CMI becomes $14V_{pp}$ when the subject keeps all electronic devices away. From this experiment, we can observe that the amount of coupled CMI may dynamically change in daily life, and when people get closer to the power rails, the coupled CMI becomes higher. Therefore, we propose a common-mode averaging unit (CMAU) in this design to suppress the instantaneous CMI from the environment.

Fig. 7 depicts the working principle of the CMAU. When CMI (shown in grey) and EEG signal (shown in blue) come into the circuit part from the input nodes of the IA, as shown in Fig. 7(a). Then the CMAU, which consists of the unity gain buffers and two capacitors, averages out the CMI, as shown in Fig. 7(b). The buffers provide a high impedance node for the CMAU part to avoid the interference coupled back to the input side. The averaged CMI is sent to the circuit ground of the IA, as shown in Fig. 7(c). Since an on-chip power management unit (PMU) is implemented, the averaged CMI in the circuit ground will be passed to the supply rail. Therefore, the averaged

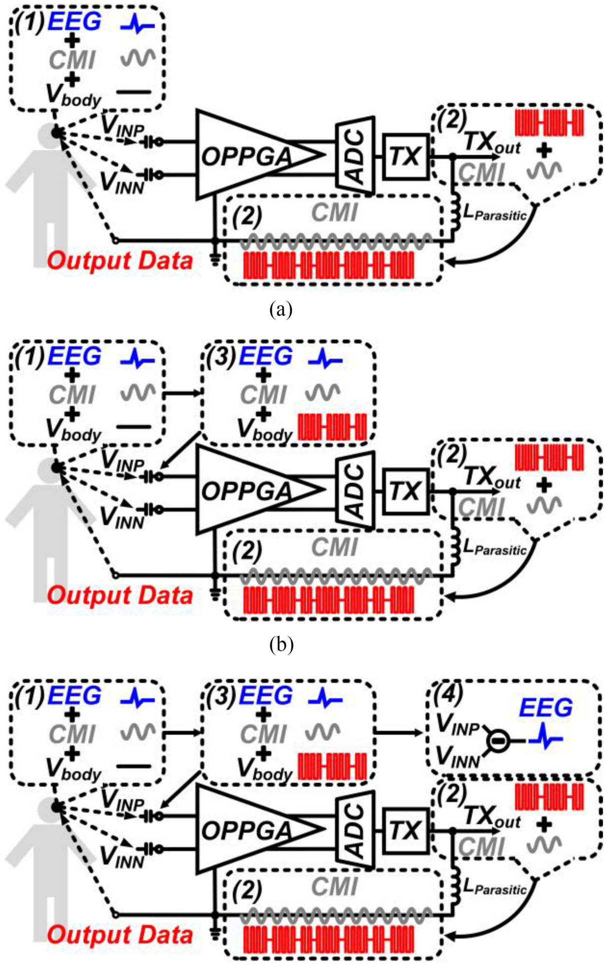

(a)

(b)

(c)

Fig. 8. Working principle of localized potential matching technique: (a) signal amplification and digitization; (b) TX transmission; (c) CMI and body potential cancellation.

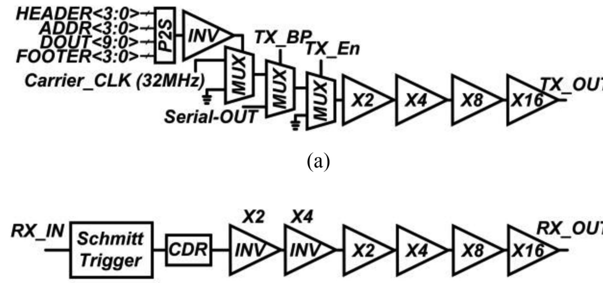

(a)

(b)

Fig. 9. The schematic of BCC blocks: (a) TX with P2S encoder; (b) RX block.

CMI is dynamically coupled to the circuit ground and supply. Moreover, to avoid ESD latch-up, due to the huge instantaneous CMI, the ESD cells' supply/ground is tied to the main chip's supply/ground, respectively. Then the CMI coupled to the chip's supply/ground will be the same as the environmental CMI, so the bio-potential signal remains without the crosstalk from CMI.

D. Localized Potential Matching

To reduce the ground electrode as well as the transmission wire, the localized potential matching technique is proposed. The working principle of the localized potential matching is shown in Fig. 8. In step (1), the EEG signal is sensed between the two inputs of IA (V_{INP} and V_{INN}), coming with the CMI and the body potential, which is amplified and digitized by the OPPGA and ADC, respectively. Thereafter the digital signal is transmitted by the TX to the transmission layer of the active concentric electrode through the coupling inductance L_P (75 nH) in step (2), as shown in Fig. 8 (a). The TX signal ($1.2V_{pp}$) is sent into the human body around the recording area and forces the body's potential in this area to be the same as the TX signal, shown in Fig. 8 (b). Hence the signal sensed by V_{INP} is the sum of the EEG signal, CMI, and TX signal, while the negative input is connected with the transmission layer, so the signal sensed by V_{INN} is the CMI and TX signal. Therefore, the only signal amplified by the OPPGA is the EEG signal, as shown in Fig. 8 (c). Moreover, since the TX signal is at 40 MHz, which is far beyond the bandwidth of the proposed IA ($f_{corner} < 150$ Hz), the TX signal will not saturate the IA's output. With the proposed localized potential matching technique, the system can transmit the TX signal while concurrently recording the EEG signal. Therefore, the EEG signal can be recorded without the ground electrode and achieves the concurrent recording/transmitting.

E. BCC TX and RX

The schematic of the BCC TX is shown as Fig. 9(a). A parallel-to-serial encoder is applied to convert the 10-bit parallel output from the ADC to the encoded bitstream. A 4-bit header and a 4-bit footer are used to encode the bitstream, and there is a 4-bit address used to differentiate outputs from various active concentric electrodes. The P2S encoder serializes the 4-bit header, 4-bit footer, 4-bit address, and 10-bit digitized signal from ADC, so the entire active concentric electrode system supports up to 16 channels' communication. Moreover, the TX_BP provides the bypass function for the TX part. The encoded signal can be directly sent out when the TX_BP is enabled. Once the TX_En is high, the TX part turns to sleep mode, and output will be kept to ground. The output of the TX part is based on OOK modulation. The active "high" is modulated to be a 40 MHz pulse while the active "low" is kept to ground and the modulated signal will be buffered-out.

The BCC RX consists of a Schmitt trigger, a clock data recovery (CDR) circuit, and the output buffers, as shown in Fig. 9(b). When the BCC signal is transmitted by the human body and sensed by an active concentric electrode, the signal is first reconstructed as a full-swing signal by the Schmitt trigger and recovered to be the encoded bitstream by the CDR block.

III. Measurement Results

The proposed active concentric electrode was fabricated in a 0.18-μm 1P6M CMOS process. The die photo is shown in Fig. 10, and the total area of the chip is 1.6 mm^2 while the area of

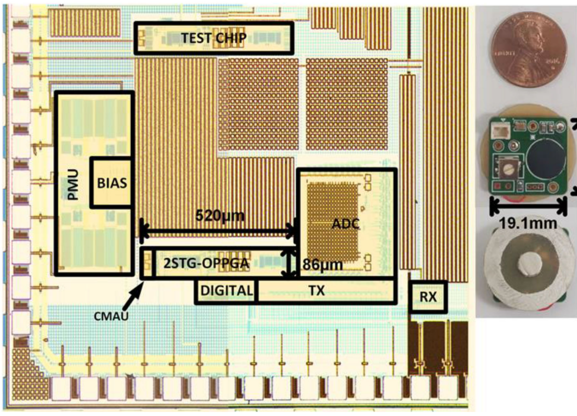

Fig. 10. Die photo of the proposed active concentric electrode and the prototype.

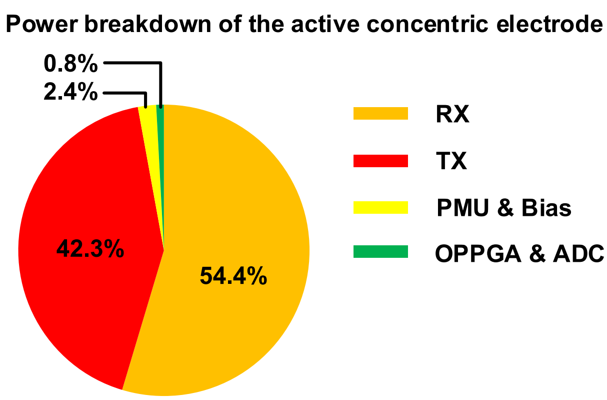

Fig. 11. Power breakdown of the proposed active concentric electrode.

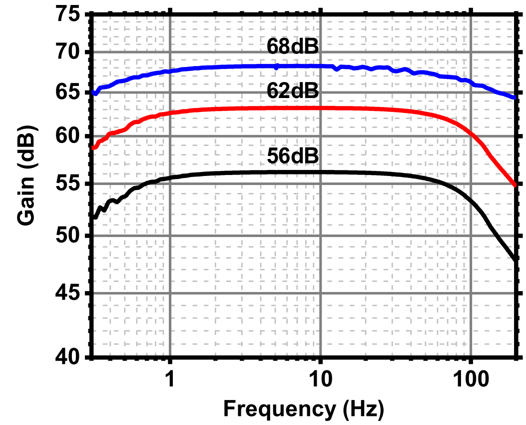

Fig. 12. The measured AC response of the AFE.

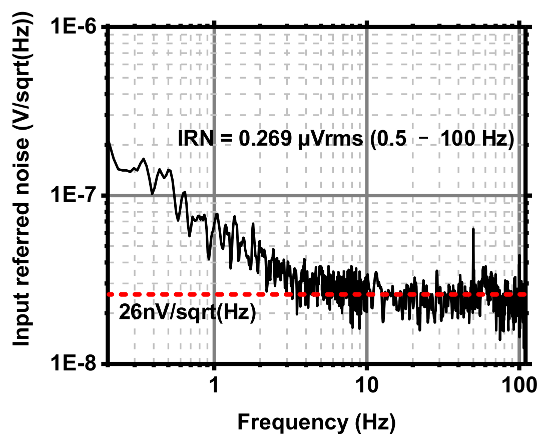

Fig. 13. The measured input-referred noise of the AFE.

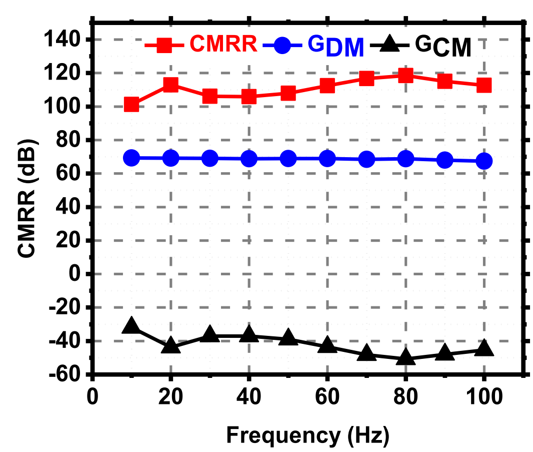

Fig. 14. The measured CMRR of the AFE.

the OPPGA is only 0.044 mm^2. The active concentric electrode size is only 18.5 mm by 19.1 mm, which is comparable to that of a US penny. The total power consumption of the proposed active concentric electrode is 1mW while the OPPGA consumes 7.4 μW, and the power breakdown of the active concentric electrode is shown in Fig. 11.

A. Performance Measurement Results

The measured AC response of the proposed OPPGA is shown in Fig. 12. With the help of the RC-DIV block, the OPPGA provides a programmable gain of 68/62/56 dB, which is controlled by the 3-bit control signal. The corresponding low/high cut-off frequencies are 0.33/140 Hz, 0.40/104 Hz and 0.38/102 Hz for 68 dB, 62 dB and 56 dB, respectively. Compared with the design values, the high pass corner is slightly higher than the simulation result due to the parasitic capacitance coupled to the input end. The measured input-referred noise is shown in Fig. 13. As the chopping stabilization is implemented to suppress the IA's flicker noise, the noise density of the proposed IA is only 26 nV/$\sqrt{}$ Hz, and the input-referred noise is only 0.269 μVrms integrated from 0.5 to 100 Hz.

By adopting the CMAU to cancel the instantaneous CMI, the measured CMRR result is shown in Fig. 14. The measured CMRR is more than 100 dB over the frequency range of 100 Hz, which is the bandwidth of the EEG signal. Moreover, with the help of CMAU and on-chip PMU, the PSRR of the IA is measured to be more than 110 dB as shown in Fig. 15.

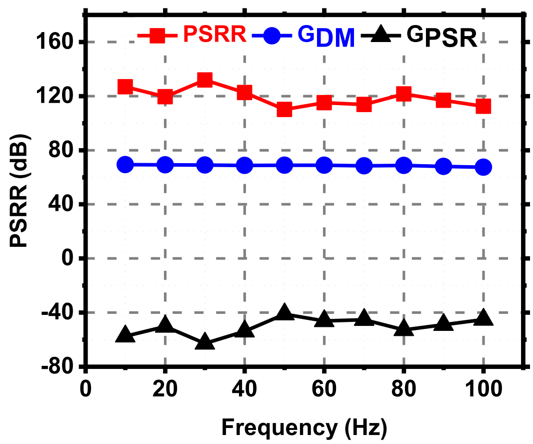

Fig. 15. The measured PSRR of the AFE.

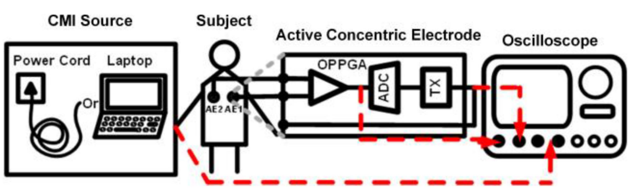

Fig. 16. Test set-up for measuring instantaneous common-mode interference (CMI) by touching laptop.

B. In-Vivo Measurement Results

The test set-up for measuring the instantaneous CMI at the working status of the proposed work is shown in Fig. 16. Since the periodical ECG signal with PQRST features is easier than the EEG signal to be recognized in the time-domain, an ECG measurement has been set up to check the system response towards instantaneous CMI. The subject who wears the active concentric electrode touches the laptop's surface to see the instantaneous CMI changes.

To verify the functionality of the CMAU block, a comparison is made between two sets of ECG recording set-up to the same subject. One set is the proposed active concentric electrode, and the other is the commercial chipset (Intan RHD 2132) [38]. For a fair comparison, the conventional 3M electrodes are used for both of the recording sets. By touching the laptop's surface, the simultaneously recorded ECG signals from both the active concentric electrode testing board and RHD 2132 are shown in Fig. 17. The recorded ECG signal on the left of the screen is from the active concentric electrode testing chip, while the right is from RHD 2132. The normal ECG waveform in the left indicates that the proposed active concentric electrode chip, which is equipped with CMAU block, withstands the huge *instantaneous and continuous* CMI injected by touching the laptop. In contrast, the commercial chipset is immediately saturated by the CMI and no useful ECG signal is shown on the right side of the screen.

To verify the amount of the instantaneous CMI suppressed by the active concentric electrode, both ECG and EEG's measurement results are shown in Fig. 18. When the subject touches a charging laptop at t = 4 s, we can observe the CMI of $51V_{pp}$ showing up instantly; even with such high instantaneous CMI,

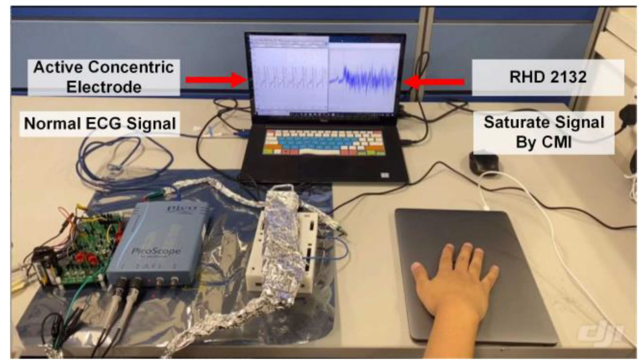

Fig. 17. Comparative testing result for active concentric electrode and Intan RHD 2132 by touching the surface of laptop.

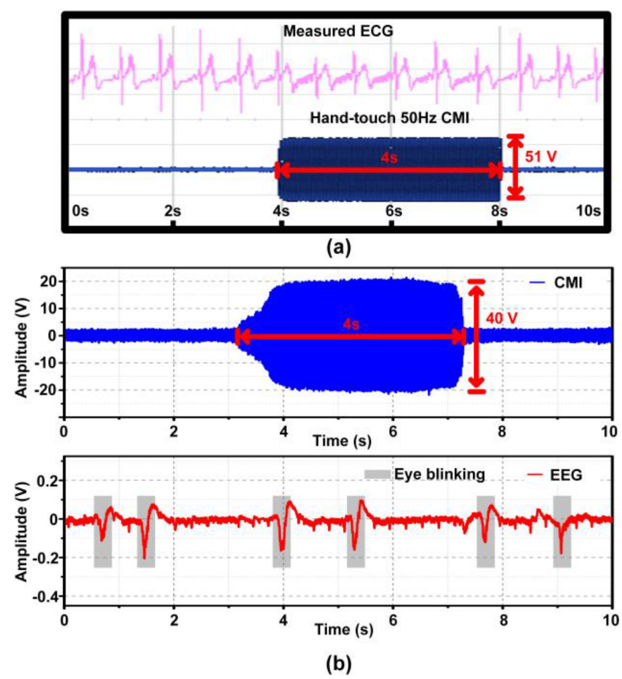

Fig. 18. Human-trial measurement result: (a) ECG recording result with the $51V_{pp}$ instantaneous CMI, (b) EEG recording result with the $40V_{pp}$ instantaneous CMI.

the ECG is successfully amplified without saturation. The EEG recording is clear to see the eye blinking despite the hand touches the power cord, coupling a CMI of $40V_{pp}$ for 4 s.

Concurrent recording/transmission of signals is another important performance required for such an active concentric electrode. As shown in Fig. 19, the proposed localized potential matching successfully shows the *concurrent* recording of the ECG signal (Fig. 19(a)) and the transmission of BCC data (Fig. 19(b)), while the concurrent recording of the EEG signal is shown in Fig. 19(c). The recovered data stream at a distance of 15 cm (electrode at the forehead to the electrode at the neck) is shown in Fig. 19(d). Therefore, the active concentric electrode fully supports concurrent signal recording/data transmitting without the ground electrode. An SNR measurement is conducted when the TX/RX distance varies. The measured

TABLE I
COMPARISON WITH THE STATE-OF-THE-ART WORKS

Parameters	ISSCC'19 [19]	ISSCC'18 [36]	VLSI'18 [37]	VLSI'18 [25]	This work
Technology	0.18 μm	0.18 μm	65 nm	65nm	0.18 μm
No. of channels	1	16	2	2	Scalable (1-16)
Active Electrode	Y	N	Y	Y	Y
Tolerance to CMI (V)	30	NA	2.8	NA	51
Instantaneous CMI Suppression	NA	NA	NA	NA	Y
Ground Electrode	N	Y	Y	Y	N
Data Transmission	Wired	Wired	Wired	BCC	BCC Network
Concurrent Recording/Transmission	N	N	N	N	Y
BCC Modulation	NA	NA	NA	Super Regenerative OOK	OOK
BCC TRX Power (μW)	NA	NA	NA	79.4	960
BCC Carrier Frequency (Hz)	NA	NA	NA	13.56M	40M
BCC Data Rate	NA	NA	NA	100kbps	512kbps
IA + PGA Area (mm^2)	0.271	0.075	1.230	1.630	0.044
Supply Voltage (V)	1.2	1.5	5	0.8	0.9/1.2
Power per IA+PGA (μW)	27.8	3.23	90	4.16	7.4
Gain (dB)	35	39.8	20/13/9/0	NA	68/62/56
Input-referred noise (μV_{rms}) (0.5 ~100 Hz)	5.05	3 (10~10kHz)	3.7	0.38	0.269
Bandwidth (Hz)	15k	10k	10k	100	100
NEF	NA	1.69	NA	3.32	2.9
CMRR (dB)	68	>110	70	>95	>100
PSRR (dB)	NA	101	NA	NA	>110
EDO Tolerance	NA	NA	Rail-to-Rail	350mV	Rail-to-Rail
Application	ECG	ECG	ECG	EEG/BCC	EEG

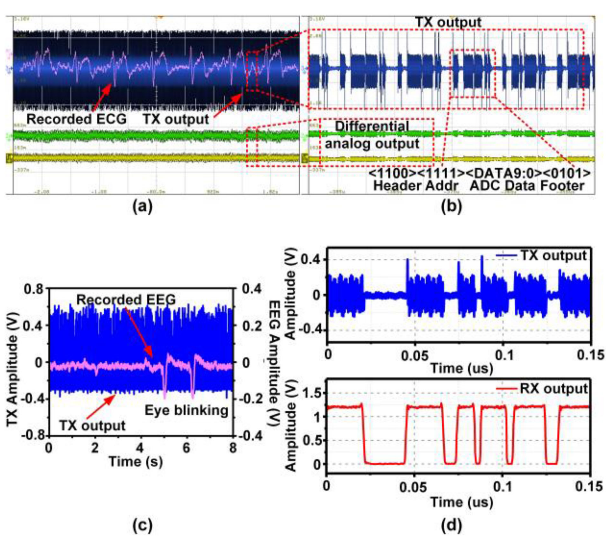

Fig. 19. Human-trial measurement results: (a) Concurrent ECG recording/BCC transmitting; (b) zoom-in view of the TX output; (c) Concurrent EEG recording/BCC transmitting; (d) BCC TX and RX output signals.

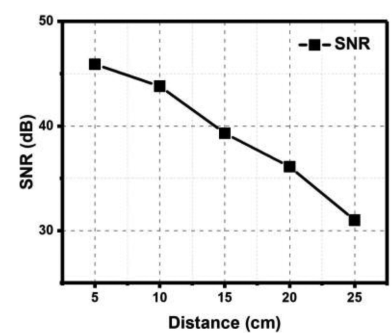

Fig. 20. Measured SNR of the received BCC RX signal vs distance.

SNR (as shown in Fig. 20) of the received signal in the RX side is inversely proportional to the distance between TX and RX.

The performance summary is shown in Table I. With the unique circuit configuration of the active concentric electrode, the presented work is the first reported so far to achieve the concurrent EEG signal recording and BCC-based data transmission. A CMAU block is implemented to support $51V_{pp}$ instantaneous CMI fluctuation and achieves 100 dB CMRR and 110 dB PSRR. Moreover, the OPPGA, equipped with RC-DIV block, only occupies 0.044 mm^2. With the help of localized potential matching technique, there is no need for ground electrode in the active concentric electrode. Therefore, the CMI coupled with the transmission wire is further reduced. The IA's power consumption is 7.4 μW, and the input-referred noise density is only 26 nV/$\sqrt{}$ Hz. The calculated NEF of the design is 2.9 and the chip supports rail-to-rail electrode dc offset tolerance.

IV. CONCLUSION

We presented an active concentric electrode for wearable EEG recording. The innovative combination of the EEG recording chip with the 3-layer concentric electrode provides a wearable EEG monitoring solution. The coin-size chip tolerates $51V_{pp}$ instantaneous CMI with the proposed CMAU block. The localized potential matching technique eliminates ground electrode and transmission wire, so the possibly coupled CMI from the environment is further reduced. The OPPGA that adopts the pseudo-resistor-based RC-DIV block provides the programmable gain and low-pass filtering, and saves the on-chip silicon area. The chip is capable of concurrent EEG recording and BCC transmission. The chip's power consumption is 7.4 μW while the input-referred noise is only 0.269 μVrms integrated from 0.5 to 100 Hz. The measured CMRR and PSRR of the IA are more than 100 dB and 110 dB, respectively.

References

[1] M. A. B. Altaf *et al.*, "A 16-channel patient-specific seizure onset and termination detection SoC with machine-learning and voltage-mode transcranial stimulation," in *IEEE Int. Solid-State Circuits Conf. Dig. Tech. Papers*, Feb. 2015, pp. 394–395.

[2] T. Tang, J. H. Park, L. Zhang, K. A. Ng, and J. Yoo, "An 8-channel 2.1 μW 0.017mm^2 0.04% gain mismatch bio-potential recording AFE using Group-chopping technique," in *Proc. IEEE Custom Integr. Circuits Conf.*, Apr. 2019, pp. 1–4.

[3] M. A. B. Altaf and J. Yoo, "A 1.83 μJ/Classification, 8-Channel, patient-specific epileptic seizure classification SoC using a non-linear support vector machine," *IEEE Trans. Biomed. Circuits Syst.*, vol. 10, no. 1, pp. 49–60, Feb. 2016.

[4] H. A. Gonzalez, S. Muzaffar, J. Yoo, and I. M. Elfadel, "BioCNN: A hardware inference engine for EEG-based emotion detection," *IEEE Access*, vol. 4, pp. 140896–140914, Aug. 2020.

[5] N. V. Helleputte *et al.*, "A 160 μA biopotential acquisition IC with fully integrated IA and motion artifact suppression," *IEEE Trans. Biomed. Circuits Syst.*, vol. 6, no. 6, pp. 552–561, Dec. 2012.

[6] A. Veeravalli, E. Sánchez-Sinencio, and J. Silva-Martínez, "A CMOS transconductance amplifier architecture with wide tuning range for very low frequency applications," *IEEE J. Solid-State Circuits*, vol. 37, no. 6, pp. 776–781, Aug. 2002.

[7] M. A. Pertijs and W. J. Kindt, "A 140 dB CMRR current-feedback instrumentation amplifier employing ping-pong auto-zeroing and chopping," *IEEE J. Solid-State Circuits*, vol. 45, no. 10, pp. 2044–2056, Sep. 2010.

[8] R. Pallas-Areny and J. G. Webster, "Common mode rejection ratio in differential amplifiers," *IEEE Trans. Instrum. Meas.*, vol. 40, no. 4, pp. 669–676, Aug. 1991.

[9] J. Xu *et al.*, "A 160 μW 8-channel active electrode system for EEG monitoring," in *IEEE Int. Solid-State Circuits Conf. Dig. Tech. Papers*, pp. 300–302, Feb. 2011.

[10] J. Xu *et al.*, "A wearable 8-channel active-electrode EEG/ETI acquisition system for body area networks," *IEEE J. Solid-State Circuits*, vol. 49, no. 9, pp. 2005–2016, Sep. 2014.

[11] B. B. Winter and J. G. Webster, "Driven-right-leg circuit design," *IEEE Trans. Biomed. Eng.*, vol. 1, pp. 62–66, Jan. 1983.

[12] M. A. Haberman and E. M. Spinelli, "A multi-channel EEG acquisition scheme based on single ended amplifiers and digital DRL," *IEEE Trans. Biomed. Circuits Syst.*, vol. 6, no. 6, pp. 614–618, Apr. 2012.

[13] E. M. Spinelli, N. H. Martinez, and M. A. Mayosky, "A transconductance driven-right-leg circuit," *IEEE Trans. Biomed. Eng.*, vol. 46, no. 12, pp. 1466–1470, Dec. 1999.

[14] M. Guermandi *et al.*, "A driving right leg circuit (DgRL) for improved common mode rejection in bio-potential acquisition systems," *IEEE Trans. Biomed. Circuits Syst.*, vol. 10, no. 2, pp. 507–517, Aug. 2015.

[15] T. Tang *et al.*, "An integrated multi-channel biopotential recording analog front-end IC with area-efficient driven-right-leg circuit," *IEEE Trans. Biomed. Circuits Syst.*, vol. 14, no. 2, pp. 297–304, Dec. 2019.

[16] K. A. Ng and Y. P. Xu, "A low-power, high CMRR neural amplifier system employing CMOS inverter-based OTAs with CMFB through supply rails," *IEEE J. Solid-State Circuits*, vol. 51, no. 3, pp. 724–737, Mar. 2016.

[17] T. Tang, W. L. Goh, L. Yao, and Y. Gao, "A TDM-Based 16-Channel AFE ASIC with enhanced system-level CMRR for wearable EEG recording with dry electrodes," *IEEE Trans. Biomed. Circuits Syst.*, vol. 14, no. 3, pp. 516–524, Mar. 2020.

[18] C. Fonseca *et al.*, "A novel dry active electrode for EEG recording," *IEEE Trans. Biomed. Eng.*, vol. 54, no. 1, pp. 162–165, Dec. 2006.

[19] N. Koo and S. H. Cho, "A 27.8 μW biopotential amplifier tolerant to 30 V pp common-mode interference for two-electrode ECG recording in 0.18 μm CMOS," in *IEEE Int. Solid-State Circuits Conf. Dig. Tech. Papers*, Feb. 2019, pp. 366–368.

[20] L. Zhang, T. Tang, J. H. Park, and J. Yoo, "A 0.012 mm^2, 1.5 GΩ Z_{IN} intrinsic feedback capacitor instrumentation amplifier for bio-potential recording and respiratory monitoring," in *Proc. IEEE Asian Solid-State Circuits Conf.*, Nov. 2019, pp. 301–304.

[21] J. H. Park *et al.*, "A 15-Channel orthogonal code chopping instrumentation amplifier for area-efficient, low mismatch bio-signal acquisition," *IEEE J. Solid-State Circuits*, vol. 55, no. 10, pp. 2771–2780, Oct. 2020.

[22] M. Sawan *et al.*, "Wireless recording systems: From non-invasive EEG-NIRS to invasive EEG devices," *IEEE Trans. Biomed. Circuits Syst.*, vol. 7, no. 2, pp. 186–195, Apr. 2013.

[23] W. Saadeh, M. A. B. Altaf, H. Alsuradi, and J. Yoo, "A pseudo OFDM with miniaturized FSK demodulation body-coupled communication transceiver for binaural hearing aids in 65 nm CMOS," *IEEE J. Solid-State Circuits*, vol. 52, no. 3, pp. 757–768, Mar. 2017.

[24] W. Saadeh, M. A. B. Altaf, H. Alsuradi, and J. Yoo, "A 1.1 mW ground effect-resilient body-coupled communication transceiver with pseudo OFDM for head and body area network," *IEEE J. Solid-State Circuits*, vol. 52, no. 10, pp. 2690–2702, Oct. 2017.

[25] J. Lee *et al.*, "A 0.8 V 82.9 μW in-ear BCI controller system with 8.8 PEF EEG instrumentational amplifier and wireless BAN transceiver," *IEEE Symp. VLSI Circuits*, pp. 123–124, Jun. 2018.

[26] J. Li *et al.*, "Human-body-coupled power-delivery and ambient-energy-harvesting ICs for a full-body-area power sustainability," *IEEE Int. Solid-State Circuits Conf. Dig. Tech. Papers*, vol. 63, pp. 514–516, Feb. 2020.

[27] J. Li *et al.*, "Body-Area Powering with Human Body-Coupled Power Transmission and Energy Harvesting ICs," *IEEE Trans. Biomed Circuits Syst.* (accepted for publication), doi: 10.1109/TBCAS.2020.3039191.

[28] J. Jang *et al.*, "Wireless body-area-network transceiver and low-power receiver with high application expandability," *IEEE J. Solid-State Circuits*, vol. 55, no. 10, pp. 2781–2789, 2020.

[29] S. Maity *et al.*, "Bio-physical modeling, characterization, and optimization of electro-quasistatic human body communication," *IEEE Trans. Biomed. Eng.*, vol. 66, no. 6, pp. 1791–1802, 2018.

[30] S. Maity *et al.*, "BodyWire: A 6.3-pJ/b 30-Mb/s− 30-dB SIR-tolerant broadband interference-robust human body communication transceiver using time domain interference rejection," *IEEE J. Solid-State Circuits*, vol. 54, no. 10, pp. 2892–2906, 2019.

[31] J. Mao *et al.*, "A five-tissue-layer human body communication circuit model tunable to individual characteristics," *IEEE Trans. Biomed. Circuits Syst.*, vol. 12, no. 2 pp. 303–312, Apr. 2018.

[32] B. Zhao *et al.*, "A low-power compact IEEE 802.15. 6 compatible human body communication transceiver with digital sigma–delta IIR mask shaping," *IEEE J. Solid-State Circuits*, vol. 54, no. 2, pp. 346–357, 2018.

[33] T. Tang *et al.*, "EEG dust: A BCC-based wireless concurrent recording/transmitting concentric electrode," in *Proc. IEEE Int. Solid-State Circuits Conf. Dig. Tech. Papers*, Feb. 2020, pp. 516–518.

[34] F. Zhang, J. Holleman, and B. P. Otis, "Design of ultra-low power biopotential amplifiers for biosignal acquisition applications," *IEEE Trans. Biomed. Circuits Syst.*, vol. 6, no. 4, pp. 344–355, 2012.

[35] J. Kim and H. Ko, "1.2 V low-power CMOS chopper-stabilized analog front-end IC for glucose monitoring," *IEEE Sensors J.*, vol. 16, no. 17, pp. 6517–6518, 2016.

[36] S. Lee *et al.*, "A 110 dB-CMRR 100 dB-PSRR multi-channel neural-recording amplifier system using differentially regulated rejection ratio enhancement in 0.18 μm CMOS," in *Proc. IEEE Int. Solid-State Circuits Conf. Dig. Tech. Papers*, Feb. 2018, pp. 472–474.

[37] M. Chen *et al.*, "A 400 GΩ input-impedance, 220 mVpp linear-input-range, 2.8 Vpp CM-interference-tolerant active electrode for non-contact capacitively coupled ECG acquisition," in *Proc. IEEE Symp. VLSI Circuits*, 2018, pp. 129–130.

[38] Intan Technologies: RHD electrophysiology Amplifier Chips. [Online] Available: https://intantech.com/products_RHD2000.html

Tao Tang (Member, IEEE) received the B.S. degree from Wuhan University, Wuhan, China, in 2012, and the M.S. and Ph.D. degrees from Nanyang Technological University, Singapore, in 2013 and 2018, respectively, all in electrical engineering. From 2012 to 2017, he was an attached Research Student with the Institute of Microelectronics (IME), Agency for Science, Technology and Research (A∗STAR), Singapore. He has been a Research Fellow with National University of Singapore, Singapore, since 2017. His research interests include low-noise, high-performance readout circuits and system for biomedical applications and brain–machine interfaces.

Long Yan (Senior Member, IEEE) received the Ph.D. degree in electrical engineering from the Korea Advanced Institute of Science and Technology (KAIST), Daejeon, South Korea, in 2011. In 2010, he was with the Microsystems Technology Laboratory, Massachusetts Institute of Technology (MIT), Cambridge, MA, USA, as a Visiting Student. From 2011 to 2014, he has been with IMEC, Belgium, as a Senior Scientist. His research at IMEC has focused on the development of low-power mixed-mode circuits for wearable and implantable applications. He is currently with Samsung Electronics, Hwaseong, South Korea as a principal member of the technical staff, where he is leading advanced sensor developments for mobile and wearable devices. Since 2015, he has been serving on the technical program committee of the IEEE International Solid-State Circuit Conference (ISSCC). He is the Chair of Far East Regional Committee of ISSCC 2021.

Jeong Hoan Park (Member, IEEE) received the B.S. and Ph.D. degrees from the School of Electrical Engineering and Computer Science, Seoul National University, Seoul, South Korea, in 2011 and 2017, respectively. He has held a Research Fellow position with the Electrical and Computer Engineering Department, National University of Singapore (NUS), Singapore, from 2017 to 2020. He is currently a Staff Engineer with the DRAM Design team, Samsung Electronics, Hwaseong, South Korea. His main research topics are developing low-power and low-noise multichannel bio-signal acquisition and the neural prosthesis with neuromorphic processing SoC. Also, he is interested in high bandwidth memory (HBM).

Han Wu (Student Member, IEEE) received the B.Eng. degree in electronic science and technology, the M.E. degree in microelectronics and solid-state electronics from the College of Opto-electronic Engineering, Chongqing University, Chongqing, China, in 2013 and 2016. He has been working toward the Ph.D. degree with the Electrical and Computer Engineering Department, National University of Singapore, Singapore, since 2017. His research focuses on energy-efficient high-speed links, ultra low-power System-on-Chip design and MEMS sensor interface circuit design.

Lian Zhang (Student Member, IEEE) received the B.E. degree from the School of Electrical and Electronic Engineering, Nanyang Technological University, Singapore, in 2016. She is currently working toward the Ph.D. degree with the Department of Electrical and Computer Engineering, National University of Singapore, Singapore. Her research focuses on low-power and low-noise analog instrumentation, area-efficient data conversion, and mixed-signal system implementation for bio-medical applications.

Jiamin Li (Student Member, IEEE) received the B.Eng. degree in electrical engineering from the National University of Singapore (NUS), Singapore, in 2017. She is currently working toward the Ph.D. degree with the Department of Electrical and Computer Engineering, NUS. Her current research interests include power management and mixed-signal integrated circuits and systems for low-power wireless wearable platforms. She was a recipient of the Student Travel Grant Award at ISSCC 2020.

Yilong Dong (Student Member, IEEE) received the B.Eng. degree in electrical engineering from the Dalian University of Technology (DUT), Dalian, China, in 2017. He is currently working toward the Ph.D. degree with the Department of Electrical and Computer Engineering, National University of Singapore (NUS), Singapore. His current research interests include body area power transfer circuits and systems for wireless wearable platforms.

Benjamin Ho Yin Lee (Student Member, IEEE) received the Diploma (with Merit) in electrical and electronic engineering from Singapore Polytechnic (SP), Singapore, in 2015. He is currently working toward the B.Eng. degree with the Department of Electrical and Computer Engineering, National University of Singapore (NUS), Singapore. His current research interests include biomedical applications and wearable technologies.

Jerald Yoo (Senior Member, IEEE) received the B.S., M.S., and Ph.D. degrees from the Department of Electrical Engineering, Korea Advanced Institute of Science and Technology (KAIST), Daejeon, South Korea, in 2002, 2007, and 2010, respectively. From 2010 to 2016, he was with the Department of Electrical Engineering and Computer Science, Masdar Institute, Abu Dhabi, United Arab Emirates, where he was an Associate Professor. From 2010 to 2011, he was also with the Microsystems Technology Laboratories (MTL), Massachusetts Institute of Technology (MIT) as a Visiting Scholar. Since 2017, he has been with the Department of Electrical and Computer Engineering, National University of Singapore, Singapore, where he is currently an Associate Professor. He has pioneered research works on low-energy body-area-network (BAN) for communication / powering and wearable body sensor networks using the planar-fashionable circuit board for a continuous health monitoring system. He authored book chapters in *Biomedical CMOS ICs* (Springer, 2010), *Enabling the Internet of Things—From Circuits to Networks* (Springer, 2017), and *The IoT Physical Layer* (Springer, 2019). His current research interests include low-energy circuit technology for wearable bio-signal sensors, flexible circuit board platform, BAN communication and powering, ASIC for piezoelectric Micromachined Ultrasonic Transducers (pMUT), and System-on-Chip (SoC) design to system realization for wearable healthcare applications. Dr. Yoo is an IEEE Circuits and Systems Society (CASS) Distinguished Lecturer (2019–2021). He also served as the IEEE Solid-State Circuits Society (SSCS) Distinguished Lecturer (2017–2018). He was the recipient or a co-recipient of several awards: the IEEE International Symposium on Circuits and Systems (ISCAS) 2015 Best Paper Award (BioCAS Track), ISCAS 2015 Runner-Up Best Student Paper Award, the Masdar Institute Best Research Award in 2015, and the IEEE Asian Solid-State Circuits Conference (A-SSCC) Outstanding Design Award (2005). He was the founding Vice-Chair of IEEE SSCS United Arab Emirates (UAE) Chapter. Currently, he serves as a Technical Program Committee Member of the IEEE International Solid-State Circuits Conference (ISSCC), ISSCC Student Research Preview (co-chair), IEEE Custom Integrated Circuits Conference (CICC, Emerging Technologies Subcommittee Chair), and IEEE Asian Solid-State Circuits Conference (A-SSCC, Emerging Technologies and Applications Subcommittee Chair). He is also an Analog Signal Processing Technical Committee Member of IEEE Circuits and Systems Society.